

See discussions, stats, and author profiles for this publication at: <https://www.researchgate.net/publication/284205282>

# Operando Analysis of NiFe- and Fe-Oxyhydroxide Electrocatalysts for Water Oxidation: Detection of Fe<sup>+4</sup> by Mössbauer Spectroscopy

ARTICLE *in* JOURNAL OF THE AMERICAN CHEMICAL SOCIETY · NOVEMBER 2015

Impact Factor: 12.11 · DOI: 10.1021/jacs.5b10699

---

READS

40

## 8 AUTHORS, INCLUDING:



Jamie Chen

Pennsylvania State University

6 PUBLICATIONS 220 CITATIONS

[SEE PROFILE](#)



Hanfeng Liang

Xiamen University

27 PUBLICATIONS 162 CITATIONS

[SEE PROFILE](#)



Wenli Bi

Argonne National Laboratory

19 PUBLICATIONS 42 CITATIONS

[SEE PROFILE](#)



Ercan E Alp

Argonne National Laboratory

394 PUBLICATIONS 5,302 CITATIONS

[SEE PROFILE](#)

# Operando Analysis of NiFe and Fe Oxyhydroxide Electrocatalysts for Water Oxidation: Detection of $\text{Fe}^{4+}$ by Mössbauer Spectroscopy

Jamie Y. C. Chen,<sup>†</sup> Lianna Dang,<sup>†</sup> Hanfeng Liang,<sup>†</sup> Wenli Bi,<sup>‡</sup> James B. Gerken,<sup>†</sup> Song Jin,<sup>\*†</sup>  
E. Ercan Alp,<sup>\*‡</sup> and Shannon S. Stahl<sup>\*†</sup>

<sup>†</sup>Department of Chemistry, University of Wisconsin—Madison, 1101 University Avenue, Madison, Wisconsin 53706, United States  
<sup>‡</sup>Advanced Photon Source, Argonne National Laboratory, 9700 South Cass Avenue, Lemont, Illinois 60439, United States

## S Supporting Information

**ABSTRACT:** Nickel–iron oxides/hydroxides are among the most active electrocatalysts for the oxygen evolution reaction. In an effort to gain insight into the role of Fe in these catalysts, we have performed operando Mössbauer spectroscopic studies of a 3:1 Ni:Fe layered hydroxide and a hydrous Fe oxide electrocatalyst. The catalysts were prepared by a hydrothermal precipitation method that enabled catalyst growth directly on carbon paper electrodes.  $\text{Fe}^{4+}$  species were detected in the NiFe hydroxide catalyst during steady-state water oxidation, accounting for up to 21% of the total Fe. In contrast, no  $\text{Fe}^{4+}$  was detected in the Fe oxide catalyst. The observed  $\text{Fe}^{4+}$  species are not kinetically competent to serve as the active site in water oxidation; however, their presence has important implications for the role of Fe in NiFe oxide electrocatalysts.

The oxygen evolution reaction (OER) is one of the main bottlenecks in photoelectrochemical solar energy conversion into chemical fuels.<sup>1</sup> Oxides/hydroxides containing both Ni and Fe have emerged as the most active electrocatalysts under alkaline conditions, and numerous studies show that they exhibit substantially higher activity than oxides containing only Ni or Fe.<sup>2</sup> In a broad survey of trimetallic oxides, we recently observed that oxides containing Ni, Fe, and a third metal (Al, Ga, Mo, among others) are even more active.<sup>3,4</sup> In an effort to begin probing the mechanistic basis for the synergistic effects of the different metals in these catalysts, we elected to initiate our studies on compositionally simpler NiFe oxide catalysts. NiFe oxide catalysts have been the subject of substantial historical<sup>5</sup> and contemporary<sup>2a,b,6</sup> investigation in the context of alkaline electrolysis and battery (e.g., NiCd) applications;<sup>7,8</sup> however, the origin of the synergy between Ni and Fe in these materials continues to be debated. Recent studies by the groups of Boettcher and Bell are particularly pertinent to the present study because of their investigation of NiFe oxide electrocatalysts under OER conditions. Boettcher and co-workers demonstrated that incorporation of Fe into a NiOOH lattice enhances the oxide conductivity, although they further showed that this effect is insufficient to explain the dramatic enhancement of catalytic activity.<sup>6e</sup> Friebel, Bell, and co-workers performed a thorough investigation of NiFe oxide electrocatalysts via operando X-ray absorption spectroscopy (XAS).<sup>7d</sup> From the data, they concluded that Fe remains

largely, if not entirely, in the  $\text{Fe}^{3+}$  oxidation state under the reaction conditions. In the same report, computational studies by Nørskov and co-workers implicated  $\text{Fe}^{3+}$  species as the active sites for water oxidation. Mössbauer spectroscopy provides a unique means by which to probe the Fe sites in these catalysts. An early study by Corrigan investigated a NiFe catalyst at an applied potential suitable to oxidize  $\text{Ni}^{2+}$  but insufficient to promote water oxidation.<sup>8a</sup> A decrease in the Fe Mössbauer isomer shift ( $\delta$ ), from 0.32 to 0.22 mm/s, was attributed to partial transfer of electron density away from  $\text{Fe}^{3+}$  species upon oxidation of the Ni centers.<sup>8</sup> The present study builds on this earlier work by using Mössbauer spectroscopy to probe a layered NiFe hydroxide electrocatalyst under active OER conditions. The results are compared to those obtained with a hydrous Fe oxide electrocatalyst. The data provide direct evidence for the formation of  $\text{Fe}^{4+}$  in the NiFe catalyst, while no  $\text{Fe}^{4+}$  is observed in the Fe oxide catalyst. These results offer unique insight into the synergistic roles of Ni and Fe in electrocatalytic water oxidation.

NiFe layered double hydroxide (LDH) catalyst precursors are readily prepared via co-precipitation and hydrothermal synthesis as powders;<sup>9</sup> however, interfacing these materials with an electrode typically requires a polymer binder, such as Nafion. The resulting composite lacks direct electrical contact with the electrode and often exhibits poor mechanical stability, especially under OER conditions. Cathodic deposition of NiFe hydroxides often results in materials contaminated with metallic Fe and Ni,<sup>7d</sup> and we observed similar complications in our initial studies using metal sulfate precursors (Figure S1, Supporting Information). To overcome these synthetic limitations, we developed a protocol that enabled the preparation of Ni, Fe, and NiFe hydroxides directly on conductive carbon paper substrates.<sup>10</sup> Carbon paper provides a high surface area for oxide growth and has minimal contribution to any background signal during Mössbauer measurements. The catalyst synthesis was carried out anaerobically by heating hydrates of  $\text{Ni}(\text{NO}_3)_2$  and/or  $\text{FeSO}_4$  at 100 °C with hydrophilic carbon paper (<0.5 mm thick) in glass vials (see Supporting Information). The use of an  $\text{Fe}^{2+}$  salt under anaerobic condition was crucial to ensure controlled precipitation of  $\text{Fe}(\text{OH})_2$ , which has a  $K_{\text{sp}}$  more compatible with  $\text{Ni}(\text{OH})_2$  than  $\text{Fe}^{3+}$  salts. Triethanolamine and urea were

Received: October 13, 2015

employed as an Fe-chelating agent and an in situ source of ammonia, respectively. For the catalyst-coated electrodes (cf. Figure 1, inset), powder X-ray diffraction (PXRD) patterns

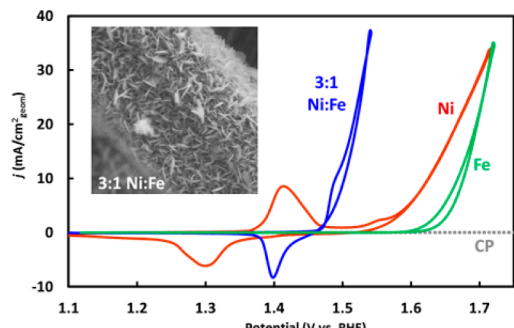


**Figure 1.** CVs of Ni (red), 3:1 Ni:Fe (blue), and Fe (green) oxyhydroxide catalysts; carbon paper (CP) background scan in gray. CVs were taken at a scan rate of 10 mV/s. Inset: SEM image of the 3:1 Ni:Fe LDH on the CP electrode.

revealed the presence of (003) and (006) basal plane peaks and confirmed the layered structure of the NiFe hydroxide catalyst (Figure S4a), while elemental mapping showed a homogeneous distribution of Fe throughout the material (Figure S6). No diffraction pattern was observed for the Fe oxide catalyst coated electrode, suggesting either a lack of sufficient material or that it is amorphous (Figure S4b).

Cyclic voltammograms (CVs) were obtained to compare the Ni, Fe, and 3:1 Ni:Fe catalysts (Figure 1). The NiFe catalyst has an onset potential for OER below 1.5 V, while the onset potentials for the Ni and Fe catalysts are 100–150 mV higher. The Ni catalyst exhibits a quasireversible  $\text{Ni}^{2+}/\text{Ni}^{3+}$  redox feature at  $E_{1/2} \approx 1.35$  V. Introduction of Fe into the Ni oxide material results in a positive shift of this feature, as expected from previous reports.<sup>5,6d,e</sup> The anodic wave of the 3:1 NiFe catalyst is nearly merged with the catalytic wave; however, a distinct cathodic feature is evident. The Fe catalyst exhibits the highest onset potential, and no redox features other than the catalytic wave were observed.<sup>11</sup>

An electrochemical cell for operando Mössbauer measurements was constructed using Delrin, an inexpensive, easily machined material with minimal  $\gamma$ -ray absorption (Figure 2). Thin windows ( $\sim 0.6$  mm thick, 8 mm diameter) were carved into both walls of the anode compartment to align with the  $\gamma$ -ray source and detector. The width of the anode compartment

was restricted to 5 mm to avoid excess attenuation of the  $\gamma$ -rays (50% transmittance with 5 mm of water). This width allowed the use of two electrodes to enhance the Mössbauer signal during operando measurements. A pump was used for continuous circulation of 95 mL of 0.1 M KOH electrolyte during data acquisition.

$^{57}\text{Fe}$ -enriched NiFe and Fe catalysts were prepared on carbon paper electrodes according to the protocol described above (see Supporting Information for details), and CVs were recorded in the operando cell prior to recording Mössbauer spectroscopic data (Figure 3a). Although the higher catalyst loading and current densities resulted in poor  $iR$  compensation relative to the traditional cell, the onset potentials observed for the NiFe- and Fe-based catalysts match those in Figure 1. An initial Mössbauer spectrum of the NiFe catalyst under open-circuit conditions (Figure 3b) reveals a doublet with an isomer shift ( $\delta$ ) of 0.34 mm/s and quadrupole splitting ( $\Delta$ ) of 0.46 mm/s. No change in the spectrum was observed upon applying a potential of 1.49 V (Figure 3c), which is at the foot of the anodic  $\text{Ni}^{2+}/\text{Ni}^{3+}$  feature and just below the onset of the catalytic activity (cf. Figure 1). When a spectrum was recorded in a region of significant catalytic OER (1.62 V applied potential), a shoulder appeared at  $\delta = -0.27$  mm/s, and the intensity reflected oxidation of approximately 12% of the Fe sites in the material (Figure 3d). Increasing the potential further to 1.76 V resulted in a growth of this oxidized Fe peak, accounting for approximately 21% of the total Fe (Figure 3e). When the potential was returned to 1.49 V, the current dropped to the baseline level observed previously at 1.49 V, but the oxidized Fe peak was still evident in the Mössbauer spectrum ( $\sim 20\%$  of total Fe, Figure 3f). After the sample was maintained for 48 h in the absence of applied potential, the oxidized Fe peak was no longer present (Figure 3g).

A similar set of experiments was performed with  $^{57}\text{Fe}$ -labeled hydrous Fe oxide as the electrocatalyst. In this case, the Mössbauer spectrum remained the same under all conditions, ranging from open-circuit to applied potentials of 1.62 and 1.76 V (Figure 3h–j). In each case, the spectrum revealed a doublet ( $\delta = 0.36$ –0.37 mm/s,  $\Delta = 0.64$ –0.67 mm/s) together with a broad baseline peak centered in the same region of the spectrum.<sup>12</sup>

The doublets in the spectra of the NiFe and Fe catalysts have very similar isomer shifts. The values of  $\delta = 0.34$ –0.37 mm/s are consistent with high-spin, Jahn–Teller-distorted  $\text{Fe}^{3+}$  species, similar to those reported previously in related materials.<sup>8,13</sup> The larger quadrupole splitting evident in the Fe-only catalyst suggests the Fe sites in this catalyst have a more-distorted geometry.

The most noteworthy feature is the oxidized Fe peak that appears in the spectrum of the NiFe catalyst upon applying a potential capable of promoting water oxidation ( $> 1.5$  V). The new peak may be fit as a singlet ( $\delta = -0.27$  mm/s), as shown in Figure 3, or as a doublet ( $\delta = 0.0$  and  $\Delta = 0.58$ , cf. Figure S7), with similar goodness-of-fits (Table S2). Either set of parameters is consistent with the assignment of this “oxidized Fe” species as  $\text{Fe}^{4+}$ .<sup>14,15</sup> These data provide the first direct evidence for the formation of  $\text{Fe}^{4+}$  in NiFe oxide catalysts during OER and contrast the recent conclusions drawn from XAS studies implicating  $\text{Fe}^{3+}$  as the highest relevant oxidation state.<sup>7d</sup> The persistence of the  $\text{Fe}^{4+}$  species in this catalyst upon lowering the potential (cf. Figure 3f), however, suggests that these  $\text{Fe}^{4+}$  sites are not directly responsible for the observed catalytic activity (see further discussion below).

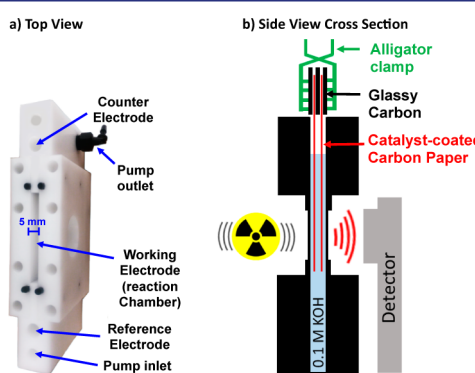


**Figure 2.** (a) Top view photograph of the operando Mössbauer-electrochemical cell. (b) Side-view cross section schematic of the cell.

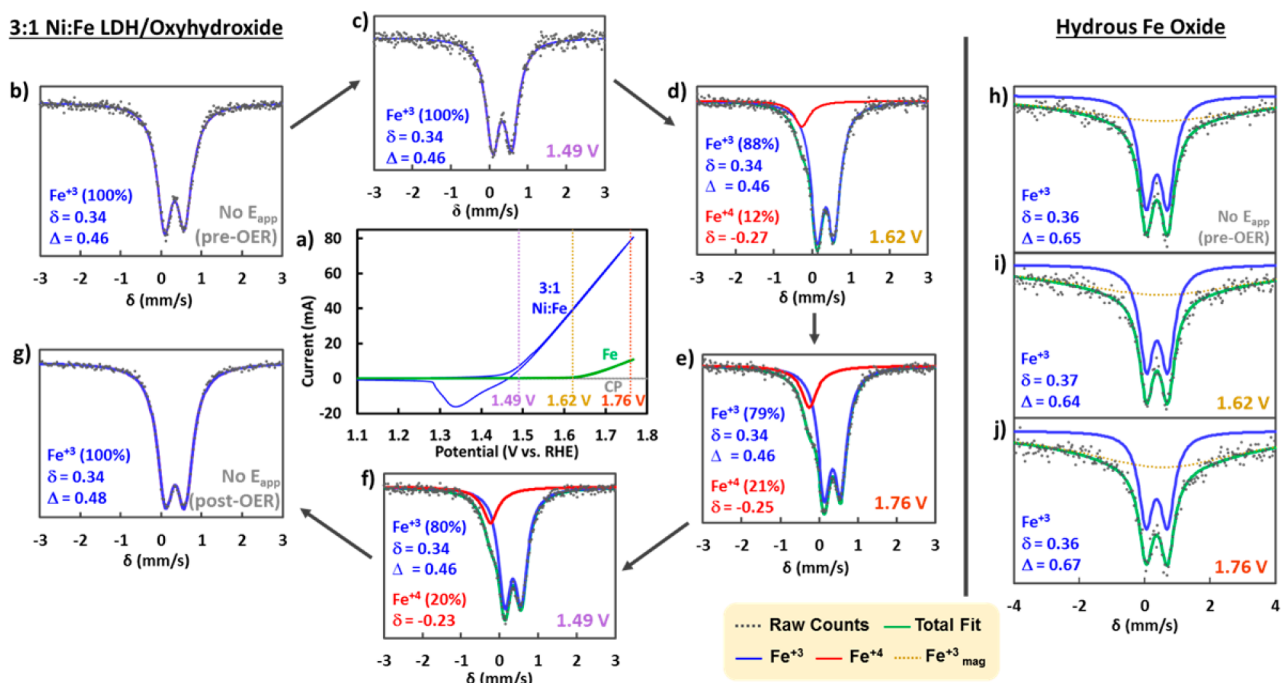


**Figure 3.** (a) CVs of NiFe layered oxyhydroxide (blue) and hydrous Fe oxide (green) electrocatalysts used for the operando experiments with Mössbauer spectra collected at open circuit (gray), at 1.49 V (purple), 1.62 V (yellow), and 1.76 V (red). CV data were recorded in the Mössbauer-electrochemical cell with a scan rate of 25 mV/s prior to Mössbauer measurements.

That no  $\text{Fe}^{4+}$  is detected in the Fe-only catalyst, even at potentials that promote catalytic OER, possibly reflects the influence of the second-coordination-sphere metal ions in the NiFe and Fe oxyhydroxide lattices.<sup>16</sup>  $\text{Ni}^{3+}$  ions have more electrons in  $\pi$ -symmetry ( $t_{2g}$ ) d-orbitals relative to  $\text{Fe}^{3+}$ . This property will increase the electron-donating ability of the  $\pi$ -symmetry lone pairs of the bridging oxygen atoms and will make the NiOOH lattice a more stable environment for high-valent metal ions, such as  $\text{Fe}^{4+}$  (Figure 4a). A complementary

spectroscopic and computational studies of Friebel, Bell, Nørskov, and co-workers attributed the catalytic activity to reactive  $\text{Fe}^{3+}$  sites.<sup>7d</sup> While our data demonstrate that the  $\text{Fe}^{4+}$  oxidation state is accessible in these catalysts, they do not distinguish Ni or Fe as the site of water oxidation. The observation of  $\text{Fe}^{4+}$  under OER conditions, however, has important mechanistic implications. We speculate that the  $\text{Fe}^{4+}$  species detected by Mössbauer spectroscopy arise from comparatively stable sites within the NiOOH lattice, such as those fully surrounded by second-coordination-sphere Ni ions (Figure 4b). If Fe sites are responsible for water oxidation activity,<sup>7d</sup> these interior high-valent Fe ions could be kinetically slow toward reaction with water, even if they have sufficiently high reduction potential to promote water oxidation (i.e., >1.5 V). On the other hand,  $\text{Fe}^{4+}$  species generated at an edge, a corner, or a related “defect” site (cf. Figure 4b) could be much more active kinetically and lead to rapid water oxidation. For example, proton-coupled electron-transfer from an  $\text{Fe}^{3+}-\text{OH}$  species could generate a highly reactive terminal  $\text{Fe}^{4+}=\text{O}$  species. Such sites are not expected to have sufficient steady-state concentration or lifetime to be detected by operando Mössbauer spectroscopy. According to this “Fe active site” mechanism, the lower overpotential of NiFe catalysts relative to Fe-only catalysts arises from the lower  $\text{Fe}^{3+/4+}$  redox potential of Fe ions at the periphery or in defect sites of the NiOOH lattice relative to similar sites in an FeOOH lattice.

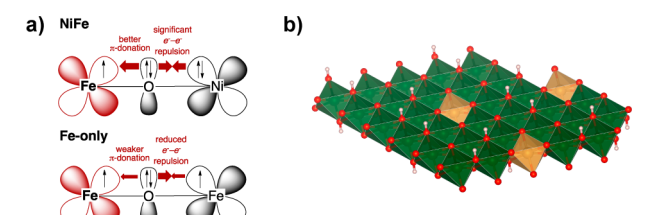


**Figure 4.** (a) Electronic effects that could rationalize the observation of  $\text{Fe}^{4+}$  in NiFe but not Fe oxide catalysts. (b) Schematic representation of a layered NiOOH lattice containing Fe ions in different sites (orange-brown).

rationale explains the increase in the  $\text{Ni}^{2+/3+}$  redox potential when  $\text{Fe}^{3+}$  ions are incorporated into Ni-LDH materials (cf. Figure 1 and previous studies<sup>2d,5,6d,e</sup>). Specifically, the presence of  $\text{Fe}^{3+}$  ions in the second coordination sphere will make bridging oxide and/or hydroxide ligands less electron-donating and thereby destabilize  $\text{Ni}^{3+}$  species in the NiOOH lattice.

It has long been assumed that Ni is the reactive site for water oxidation in NiFe oxide electrocatalysts on the basis of the high activity of Ni oxide electrocatalysts, i.<sup>6e,7a,b,8a,17</sup> However, most of these conclusions were drawn before the recent demonstration by Boettcher and co-workers that Ni oxide electrocatalysts often contain Fe contaminants,<sup>2a,6e</sup> and the recent

A “Ni active site” mechanism also seems consistent with the data. Incorporation of Fe into a NiOOH lattice will raise the  $\text{Ni}^{3+/4+}$  redox potential similar to the manner in which it raises the  $\text{Ni}^{2+/3+}$  potential (cf. Figure 1). The active Ni species are likely those at corner and/or edge sites, which will have terminal hydroxo and oxo ligands in their coordination sphere.  $\text{Ni}^{4+}$ -oxo/oxyl species with second-coordination-sphere Fe ions should be more reactive toward water oxidation relative to species entirely surrounded by Ni ions.

In conclusion, operando Mössbauer spectroscopic studies have provided the first direct evidence for the formation of  $\text{Fe}^{4+}$  in NiFe oxide catalysts during steady-state catalytic turnover. Observation of  $\text{Fe}^{4+}$  in NiFe, but not Fe-only, catalysts is attributed to the stabilizing effect of the NiOOH lattice. Although the  $\text{Fe}^{4+}$  species detected here are not directly responsible for the observed catalytic activity, future mechanistic proposals should account for the accessibility of the +4 oxidation state of iron in these catalysts. On the basis of the analysis presented above, we favor a mechanism in which water oxidation occurs at reactive (unobserved)  $\text{Fe}^{4+}$  species generated at edge, corner, or defect sites within Fe-doped NiOOH lattice.

## ASSOCIATED CONTENT

### Supporting Information

The Supporting Information is available free of charge on the ACS Publications website at DOI: [10.1021/jacs.5b10699](https://doi.org/10.1021/jacs.5b10699).

Synthesis, characterization data, experimental details, and Mossbauer spectra([PDF](#))

## AUTHOR INFORMATION

### Corresponding Authors

[\\*jin@chem.wisc.edu](mailto:jin@chem.wisc.edu)

[\\*eea@aps.anl.gov](mailto:eea@aps.anl.gov)

[\\*stahl@chem.wisc.edu](mailto:stahl@chem.wisc.edu)

### Notes

The authors declare no competing financial interest.

## ACKNOWLEDGMENTS

We thank Dr. Dennis Brown (Northern Illinois Univ.) for help during preliminary Mössbauer experiments. This research is supported by the NSF CCI grant CHE-1305124. Work at ANL was supported by DOE (DE-AC02-06CH11357 and COMPRES). S.J. thanks NSF DMR-1508558 for support. H.L. thanks the China Scholarship Council for support.

## REFERENCES

- (1) For selected reviews, see: (a) Dau, H.; Limberg, C.; Reier, T.; Risch, M.; Roggan, S.; Strasser, P. *ChemCatChem* **2010**, *2*, 724. (b) Walter, M. G.; Warren, E. L.; McKone, J. R.; Boettcher, S. W.; Mi, Q. X.; Santori, E. A.; Lewis, N. S. *Chem. Rev.* **2010**, *110*, 6446. (c) Singh, A.; Spiccia, L. *Coord. Chem. Rev.* **2013**, *257*, 2607. (d) Galán-Mascarós, J. R. *ChemElectroChem* **2015**, *2*, 37.
- (2) For leading references, see: (a) Trotochaud, L.; Ranney, J. K.; Williams, K. N.; Boettcher, S. W. *J. Am. Chem. Soc.* **2012**, *134*, 17253. (b) McCrory, C. C. L.; Jung, S. H.; Peters, J. C.; Jaramillo, T. F. *J. Am. Chem. Soc.* **2013**, *135*, 16977. (c) Smith, R. D. L.; Prévôt, M. S.; Fagan, R. D.; Trudel, S.; Berlinguette, C. P. *J. Am. Chem. Soc.* **2013**, *135*, 11580. (d) Chen, J. Y. C.; Miller, J. T.; Gerken, J. B.; Stahl, S. S. *Energy Environ. Sci.* **2014**, *7*, 1382. (e) Wang, H. T.; Lee, H. W.; Deng, Y.; Lu, Z. Y.; Hsu, P. C.; Liu, Y. Y.; Lin, D. C.; Cui, Y. *Nat. Commun.* **2015**, *6*, 7261.
- (3) (a) Gerken, J. B.; Chen, J. Y. C.; Massé, R. C.; Powell, A. B.; Stahl, S. S. *Angew. Chem., Int. Ed.* **2012**, *51*, 6676. (b) Gerken, J. B.; Shaner, S. E.; Massé, R. C.; Porubsky, N. J.; Stahl, S. S. *Energy Environ. Sci.* **2014**, *7*, 2376.
- (4) For related observations, see the following and references cited therein: (a) Singh, R. N.; Singh, J. P.; Lal, B.; Thomas, M. J. K.; Bera, S. *Electrochim. Acta* **2006**, *51*, 5515. (b) Anindita; Singh, A.; Singh, R. N. *Int. J. Hydrogen Energy* **2010**, *35*, 3243.
- (5) (a) Mlynarek, G.; Paszkiewicz, M.; Radniecka, A. *J. Appl. Electrochem.* **1984**, *14*, 145. (b) Córdoba, S. I.; Carbonio, R. E.; Teijelo, M. L.; Macagno, V. A. *Electrochim. Acta* **1987**, *32*, 749. (c) Potvin, E.; Brossard, L. *Mater. Chem. Phys.* **1992**, *31*, 311. (d) Merrill, M. D.; Dougherty, R. C. *J. Phys. Chem. C* **2008**, *112*, 3655.
- (6) (a) Hong, D.; Yamada, Y.; Nagatomi, T.; Takai, Y.; Fukuzumi, S. *J. Am. Chem. Soc.* **2012**, *134*, 19572. (b) Landon, J.; Demeter, E.; İnoğlu, N.; Keturakis, C.; Wachs, I. E.; Vasić, R.; Frenkel, A. I.; Kitchin, J. R. *ACS Catal.* **2012**, *2*, 1793. (c) Gong, M.; Li, Y.; Wang, H.; Liang, Y.; Wu, J. Z.; Zhou, J.; Wang, J.; Regier, T.; Wei, F.; Dai, H. *J. Am. Chem. Soc.* **2013**, *135*, 8452. (d) Louie, M. W.; Bell, A. T. *J. Am. Chem. Soc.* **2013**, *135*, 12329. (e) Trotochaud, L.; Young, S. L.; Ranney, J. K.; Boettcher, S. W. *J. Am. Chem. Soc.* **2014**, *136*, 6744.
- (7) (a) Corrigan, D. A. *J. Electrochem. Soc.* **1987**, *134*, 377. (b) Kim, S. H.; Tryk, D. A.; Antonio, M. R.; Carr, R.; Scherson, D. *J. Phys. Chem.* **1994**, *98*, 10269. (c) Balasubramanian, M.; Melendres, C. A.; Mini, S. *J. Phys. Chem. B* **2000**, *104*, 4300. (d) Friebel, D.; Louie, M. W.; Bajdich, M.; Sanwald, K. E.; Cai, Y.; Wise, A. M.; Cheng, M. J.; Sokaras, D.; Weng, T. C.; Alonso-Mori, R.; Davis, R. C.; Bargar, J. R.; Nørskov, J. K.; Nilsson, A.; Bell, A. T. *J. Am. Chem. Soc.* **2015**, *137*, 1305.
- (8) Mössbauer studies of layered NiFe oxide battery cathodes revealed the formation of  $\text{Fe}^{4+}$ ; however, the different conditions used in these studies relative to OER make direct comparison of the results difficult. See the following: (a) Corrigan, D. A.; Conell, R. S.; Fierro, C.; Scherson, D. A. *J. Phys. Chem.* **1987**, *91*, 5009. (b) Guerlou-Demourgues, L.; Fournes, L.; Delmas, C. *J. Electrochem. Soc.* **1996**, *143*, 3083. (c) Axmann, P.; Erdbrügger, C. F.; Buss, D. H.; Glemser, O. *Angew. Chem., Int. Ed. Engl.* **1996**, *35*, 1115.
- (9) For examples: (a) Axmann, P.; Glemser, O. *J. Alloys Compd.* **1997**, *246*, 232. (b) Xiao, T.; Tang, Y. W.; Jia, Z. Y.; Li, D. W.; Hu, X. Y.; Li, B. H.; Luo, L. *J. Nanotechnology* **2009**, *20*, 475603. (c) Abellán, G.; Coronado, E.; Martí-Gastaldo, C.; Pinilla-Cienfuegos, E.; Ribera, A. *J. Mater. Chem.* **2010**, *20*, 7451. (d) Han, Y. F.; Liu, Z. H.; Yang, Z. P.; Wang, Z. L.; Tang, X. H.; Wang, T.; Fan, L. H.; Ooi, K. *Chem. Mater.* **2008**, *20*, 360.
- (10) For a related preparation of NiCo and NiGa LDHs on carbon paper, see: (a) Liang, H. F.; Meng, F.; Cabán-Acevedo, M.; Li, L. S.; Forticaux, A.; Xiu, L. C.; Wang, Z. C.; Jin, S. *Nano Lett.* **2015**, *15*, 1421. (b) Liang, H. F.; Li, L. S.; Meng, F.; Dang, L.; Zhuo, J.; Forticaux, A.; Wang, Z. C.; Jin, S. *Chem. Mater.* **2015**, *27*, 5702.
- (11) (a) Doyle, R. L.; Lyons, M. E. G. *J. Electrochem. Soc.* **2013**, *160*, H142. (b) Wu, Y. Z.; Chen, M. X.; Han, Y. Z.; Luo, H. X.; Su, X. J.; Zhang, M. T.; Lin, X. H.; Sun, J. L.; Wang, L.; Deng, L.; Zhang, W.; Cao, R. *Angew. Chem., Int. Ed. Engl.* **2015**, *54*, 4870.
- (12) A similar broad peak has been observed in  $\delta\text{-FeOOH}$  and attributed to superparamagnetism: Pollard, R. J.; Pankhurst, Q. A. *J. Magn. Magn. Mater.* **1991**, *99*, L39.
- (13) See, for example: (a) Rossiter, M. J.; Hodgson, A. E. M. *J. Inorg. Nucl. Chem.* **1965**, *27*, 63. (b) Johnson, C. E. *J. Phys. C: Solid State Phys.* **1969**, *2*, 1996.
- (14) See ref 8 and the following: (a) Adler, P. *J. Solid State Chem.* **1994**, *108*, 275. (b) Gallagher, P. K.; Macchesney, J. B.; Buchanan, D. N. *J. Chem. Phys.* **1964**, *41*, 2429. (c) Takano, M.; Nakanishi, N.; Takeda, Y.; Naka, S.; Takada, T. *Mater. Res. Bull.* **1977**, *12*, 923.
- (15) A singlet would reflect a high-spin  $\text{Fe}^{4+}$  species in a symmetrical coordination geometry, while a doublet could arise from a low-spin  $\text{Fe}^{4+}$  species in an unsymmetrical environment. We presently favor the singlet fit on the basis of previous EXAFS studies, which reveal uniform Fe–O bond lengths in NiFe oxide electrocatalysts (refs 7b–d).
- (16) The low conductivity of FeOOH could limit the formation of  $\text{Fe}^{4+}$  sites in this material. See: (a) Burke, M. S.; Zou, S.; Enman, L. J.; Kellon, J. E.; Gabor, C. A.; Pledger, E.; Boettcher, S. W. *J. Phys. Chem. Lett.* **2015**, *6*, 3737. (b) Zou, S.; Burke, M. S.; Kast, M. G.; Fan, J.; Danilovic, N.; Boettcher, S. W. *Chem. Mater.* **2015**, DOI: [10.1021/acs.chemmater.5b03404](https://doi.org/10.1021/acs.chemmater.5b03404).
- (17) (a) Chen, Y. W. D.; Noufi, R. N. *J. Electrochem. Soc.* **1984**, *131*, 1447. (b) Bediako, D. K.; Surendranath, Y.; Nocera, D. G. *J. Am. Chem. Soc.* **2013**, *135*, 3662.

## **Supporting Information for**

### **Operando Analysis of NiFe- and Fe-Oxyhydroxide Electrocatalysts for Water Oxidation: Detection of $\text{Fe}^{+4}$ by Mössbauer Spectroscopy**

Jamie Y. C. Chen<sup>†</sup>, Lianna Dang<sup>†</sup>, Hanfeng Liang<sup>†</sup>, Wenli Bi<sup>‡</sup>, James B. Gerken<sup>†</sup>, Song Jin<sup>\*,†</sup>, E. Ercan Alp<sup>\*,‡</sup>, Shannon S. Stahl<sup>\*,†</sup>

<sup>†</sup> Department of Chemistry, University of Wisconsin - Madison, 1101 University Avenue,  
Madison, WI 53706

<sup>‡</sup> Advanced Photon Source, Argonne National Laboratory, 9700 South Cass Avenue, Lemont, IL  
60439

<b>Table of Contents</b>	<b>Page</b>
I. Mössbauer Spectra of Electrodeposited NiFe-LDH Catalyst	S2
II. Experimental Details	S3
III. Structural Characterizations	S6
IV. Mössbauer Results and Parameters	S8

## I. Mössbauer Spectra of Electrodeposited NiFe-LDH Catalyst

Our initial studies focused on NiFe-based electrocatalysts prepared via electrodeposition from solutions containing nickel and iron sulfates.<sup>S1</sup> Unfortunately, the low electrode potentials ( $\sim -0.9$  V vs. Ag/AgCl) needed to establish the pH gradient for precipitation of the metal oxides (via reduction of water to H<sub>2</sub> and hydroxide ions) causes undesired electroplating of Ni and Fe simultaneously with electrodeposition of the desired metal-hydroxides. Metallic iron is evident in the Mössbauer spectra in Figure S1a. We considered the use of metal nitrate salts as precursors for electrodeposition,<sup>S2</sup> as these should be less prone to form metallic phases. However, our attempts to confirm the lack of metallic phases in these samples using XPS depth profiling analysis were inconclusive because Ni and Fe oxides undergo preferential oxygen removal under ultra-high vacuum during the Ar<sup>+</sup> ion beam etching process (Figure S1b).<sup>S3</sup> This complication ultimately led us to pursue the development of an alternative catalyst synthesis where metallic phase formation would not be a concern.

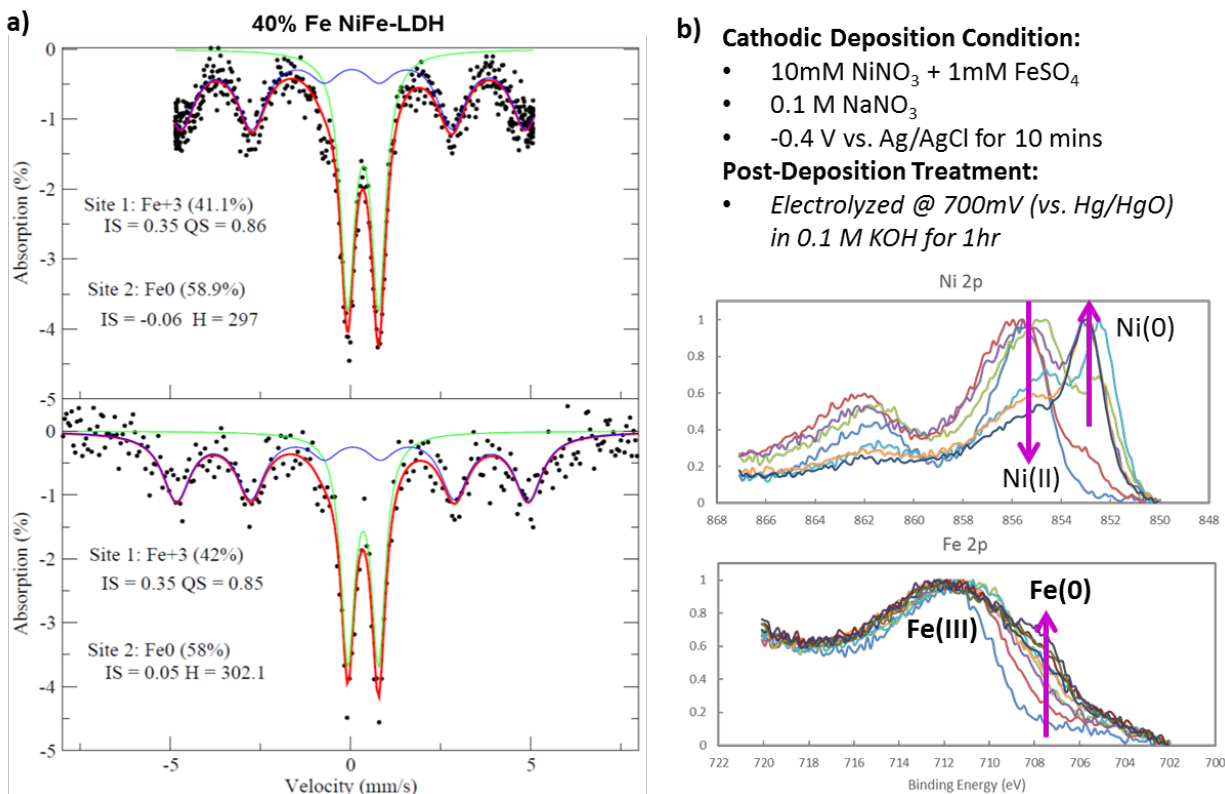


**Figure S1.** a) Mossbauer spectra of electrodeposited NiFe-LDH (40% Fe, using a metal sulfate solution) collected at two different velocities at room temperature. Sextuplet of the metallic Fe can be readily identified. b) XPS etching profile of an anodized 10% Fe NiFe-LDH film deposited from a metal nitrate solution, showing the appearance of metallic phases with increasing etching cycles.

## II. Experimental Details

### 2.1 Materials.

All chemicals were purchased from Sigma Aldrich in the highest purity available and used as received except for  $\text{FeSO}_4 \cdot 7\text{H}_2\text{O}$ .  $\text{FeSO}_4 \cdot 7\text{H}_2\text{O}$  was recrystallized and stored under  $\text{N}_2$  to avoid oxidation of  $\text{Fe}^{+2}$  to  $\text{Fe}^{+3}$ .  $^{57}\text{Fe}$  metal was purchased from ISOFLEX and converted into  $^{57}\text{FeSO}_4 \cdot 7\text{H}_2\text{O}$  (vide infra). Carbon paper (CP) was purchased from Fuel Cell Earth and was subjected to hydrophilic treatment before use (vide infra).  $\text{N}_2$  purged ultrapure de-ionized water ( $18 \text{ M}\Omega$ , Thermo-Scientific) was used to prepare all aqueous solution.  $\text{Hg}/\text{HgO}$  reference electrode (1 M KOH) and Pt mesh counter electrode (BASi Analytical Instruments) were used in all electrochemical experiments.

### 2.2 Synthesis of $^{57}\text{FeSO}_4 \cdot 7\text{H}_2\text{O}$

*Note: considerable care was taken to keep  $^{57}\text{Fe}$  from exposure to  $\text{O}_2$  throughout the entire reaction.* A 10 cm piece of Tygon tubing threaded through a rubber septum was fitted to the tip of a 50 mL plastic syringe. The syringe was filled with  $\text{N}_2$  purged 25% (v/v)  $\text{H}_2\text{SO}_4$  in a  $\text{N}_2$  purge box. A 1 g piece of  $^{57}\text{Fe}$  metal was placed into a 100 mL 3-neck round bottom flask (RBF) and kept under active  $\text{N}_2$  flow. The RBF was sealed with a rubber septum fit with a plastic syringe and 25% (v/v)  $\text{H}_2\text{SO}_4$  was slowly added to the  $^{57}\text{Fe}$  metal under active stirring and  $\text{N}_2$  flow while the flask was heated to 70 °C. After 30 mL of acid solution was added, reaction was left to stir at 70 °C or until all metal has dissolved. (Degassed  $\text{H}_2\text{O}$  was syringed into the flask if evaporation became too significant and more acid solution was added if not all metal has dissolved after 12 hours).

Once all metal was dissolved (which resulted in a very pale-green solution), a Dean-Stark trap was fitted to the RBF and the reaction temperature increased to 105-110 °C to remove  $\text{H}_2\text{O}$ . When  $\text{H}_2\text{O}$  was removed, white solids were left in the flask with  $\text{H}_2\text{SO}_4$ , which were transferred into a pipette fitted with a polypropylene frit.  $\text{N}_2$  was used to push  $\text{H}_2\text{SO}_4$  out of the syringe pipette and the solid was washed with very small amounts of cold saturated  $^{56}\text{FeSO}_4$  solution and left to dry under a  $\text{N}_2$  stream for one hour. The white solid was transferred into the  $\text{N}_2$  purge box and recrystallized as  $^{57}\text{FeSO}_4 \cdot 7\text{H}_2\text{O}$  using a minimal amount of degassed  $\text{H}_2\text{O}$  at 70 °C. This solution was subsequently sealed and transferred to a 4 °C refrigerator until green crystals appeared.

### 2.3 Hydrophilic Treatment of Carbon Paper

Each side of the carbon paper was first cleaned with oxygen plasma at 150 W power for 5 minutes. Subsequently, the carbon paper was annealed in air at 800 °C for 5 minutes to remove oxidized contaminant from the surface of the carbon paper. The resulting paper is thinner and very brittle, but no longer floats on water after some agitation.

### 2.4 Preparation of Ni/Fe-LDH Catalyst on Carbon Paper

Hydrophilic-treated carbon paper (3.5 cm × 0.8 cm) and urea (5 equiv.) were placed into a 6 mL glass vial and transferred into a purge box for catalyst synthesis. In the purge box, stock solutions of  $\text{Ni}(\text{NO}_3)_2 \cdot 6\text{H}_2\text{O}$  (1 M),  $^{57}\text{FeSO}_4 \cdot 7\text{H}_2\text{O}$  (0.1 M), and triethanolamine (TEA, 10 mM) were prepared from  $\text{O}_2$ -free de-ionized  $\text{H}_2\text{O}$ .

### Samples for Mössbauer Experiment

NiFe 3:1 LDH: 64  $\mu$ L of  $^{57}\text{FeSO}_4$  stock solution were placed into a plastic test tube, followed by 1.8 mL of TEA (1 equiv. to  $\text{Fe}^{+2}$ ) and mixed (a green  $\text{Fe}^{+2}$ -TEA complex precipitated shortly after mixing but re-dissolves during hydrothermal reaction). Subsequently, 6  $\mu$ L of  $\text{Ni}(\text{NO}_3)_2$  stock solution and 14  $\mu$ L of  $\text{H}_2\text{O}$  were added and mixed thoroughly. The entire solution mixture was transferred into a glass vial containing carbon paper (CP) and 7.2 mg of urea (5 equiv. to  $[\text{M}]_{\text{tot}}$ ) and mixed until the urea had dissolved and CP was fully wetted. The reaction mixture was then sealed under  $\text{N}_2$ , taken out of the purge box, and placed in an oven (preheated) at 100 °C for 6 hours. At the end of the hydrothermal synthesis, carbon paper was removed from the glass vials, rinsed with ultrapure water, and stored in a glass vial with just enough water to keep the carbon paper wet.

100% Fe: Follow aforementioned protocol using 180  $\mu$ L of  $^{57}\text{FeSO}_4$  stock solution, 1.8 mL of TEA stock solution, 20  $\mu$ L of  $\text{H}_2\text{O}$ , and 5.4 mg of urea, but no  $\text{Ni}(\text{NO}_3)_2$  precursor.

### Samples for Electrochemical Experiment (lower catalyst loadings)

100% Ni: Follow aforementioned protocol using 8  $\mu$ L of  $\text{Ni}(\text{NO}_3)_2$  stock solution, 1992  $\mu$ L of  $\text{H}_2\text{O}$ , and 2.4 mg of urea. No TEA was used for this sample.

100% Fe: Follow aforementioned protocol using 80  $\mu$ L of  $\text{FeSO}_4$  stock solution, 800  $\mu$ L of TEA stock solution, 1.12 mL of  $\text{H}_2\text{O}$ , and 2.4 mg of urea, but no  $\text{Ni}(\text{NO}_3)_2$  precursor.

NiFe 3:1 LDH: Follow aforementioned protocol using 8  $\mu$ L of  $\text{FeSO}_4$  stock solution, 3.2  $\mu$ L of  $\text{Ni}(\text{NO}_3)_2$  stock solution, 80  $\mu$ L of TEA stock solution, 1908  $\mu$ L of  $\text{H}_2\text{O}$ , and 1.2 mg of urea.

The concentrations used for all samples are also tabulated in Table S1 below for comparison.

**Table S1.** Specific Reaction Conditions Employed for Catalyst Synthesis.

Final Catalyst	$[\text{M}]_{\text{tot}}$ (mM)*	Ni:Fe	TEA	Urea (mg)	$\text{Vol}_{\text{tot}}$ (mL)	Temp.	Final Ratio (EDS)
100% Ni	(4)	1:0	none	5 $[\text{M}]_{\text{tot}}$ equiv.	2.0	100 °C	100% Ni
25% Fe	16 (or 2)	4:1	1 [Fe] equiv.	5 $[\text{M}]_{\text{tot}}$ equiv.	2.0	100 °C	3( $\pm 0.6$ ):1
100% Fe	9 (or 4)	0:1	1 [Fe] equiv.	5 $[\text{M}]_{\text{tot}}$ equiv.	2.0	100 °C	100% Fe

\* Values in parentheses are for electrochemical experiments

### 2.5 Characterization Methods

Powder X-ray diffraction patterns (PXRD) were recorded using a Bruker D8 Advance diffractometer equipped with the LYNXEYE detector and a Cu K $\alpha$  X-ray tube. The detector was operated at 40 kV and 40 mA and scans were collected between the range of 5° - 70° with a step size of 0.01° and an exposure time of 2-10 s per step. The recorded pattern for 3:1 NiFe-LDH on carbon paper and as free powder were in accordance with literature reports.<sup>S4</sup> No pattern can be observed for hydrous Fe-oxide grown on carbon paper. Peak assignment was not possible for pattern recorded for hydrous Fe-oxide powder due to its ill-defined nature. SEM images and EDX elemental analysis were performed using a ZEISS-LEO SUPRA 55 VP scanning electron microscope (SEM) coupled with the NORAN SYSTEM SEVEN energy dispersive X-ray spectroscopy detector (ThermoFisher-Scientific).

## 2.6 Mössbauer Measurements

Mössbauer experiments were conducted with a  $^{57}\text{Co}$  source in a Pd matrix, using a constant acceleration drive. The spectrometer was calibrated using an iron foil. The  $^{57}\text{Co}$  source used was a point source with 0.5 mm diameter, and the relative activity was 10 mCi. A VORTEX detector with 150 eV resolution was used to discriminate the 14.41 keV radiation. Data analysis was performed using in-house software. All data presented were taken at room temperature. The samples were prepared from fully enriched  $^{57}\text{FeSO}_4 \cdot 7\text{H}_2\text{O}$ .

Ex-situ measurements were collected by stacking 4 wet catalyst/CP pieces. The catalyst/CP pieces were kept wet during acquisition by placement in a small plastic bag with a couple drops of water. The plastic bag was subsequently taped onto the sample holder. Typical acquisition time ranged from 18-24 hours. 2 catalyst/CP pieces were used for operando measurements.

The cell was snuggly positioned between the source and the detector inside a lead cage. The pump and the potentiostat were positioned outside the cage, where a small opening on the lead cage (away from the source) guided the pump tubing and potentiostat leads inside to the cell (Fig. S2). The cell was replenished with fresh 0.1 M KOH solution after data collection at each condition was completed.

The working electrode assembly was prepared as follows: the top of each catalyst/CP piece was securely sandwiched between two thin strip of Cu and wrapped securely using white Teflon tape. The uncovered portion of the Cu strip was then sandwiched between pieces of glassy carbon electrode (1 mm thick), which was tightly clamped with a large alligator clamp. This entire working electrode assembly (Fig. S3) was then connected to the potentiostat by clamping the working electrode clip on the large alligator clamp. Two pieces of catalyst/CP were used in all operando experiments.

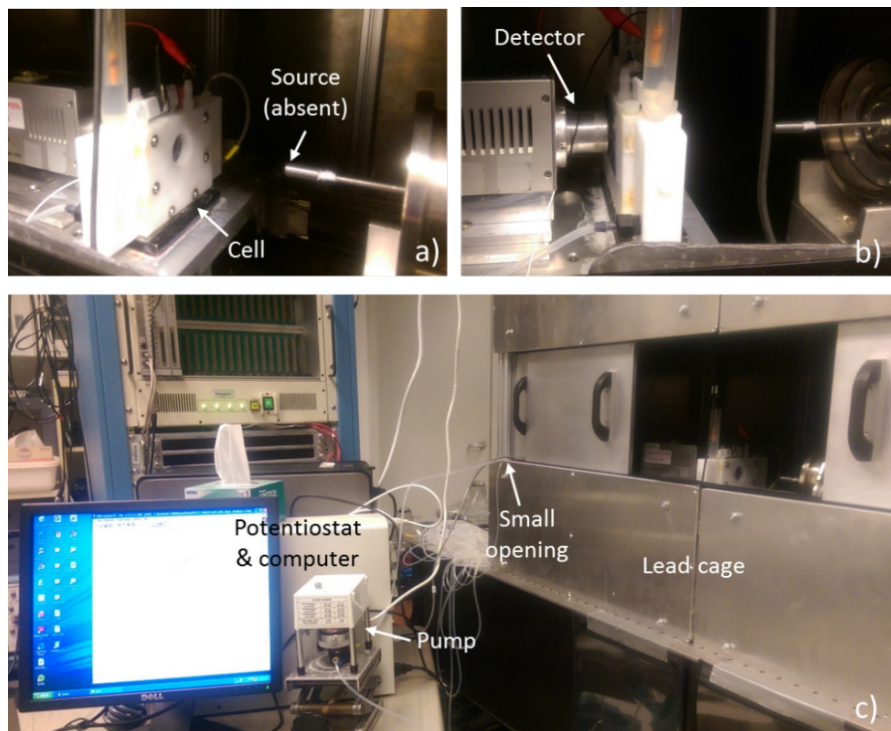


**Figure S2.** View of the experimental setup for operando Mössbauer experiment from the a) source side, b) detector side, and c) outside the lead cage.

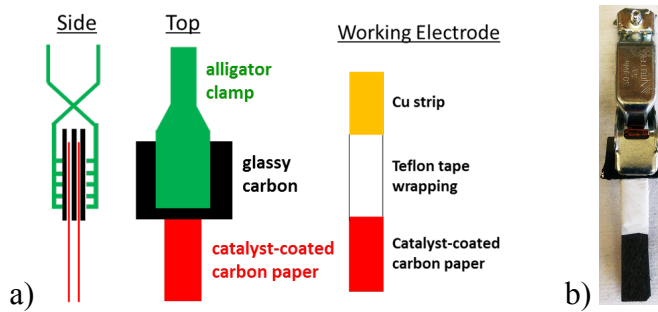


**Figure S3.** (a) Schematic representation of the working electrode assembly. (b) Photograph of the working electrode assembly used in operando Mössbauer measurements.

### III. Structural Characterizations

#### 3.1 Powder X-ray Diffraction

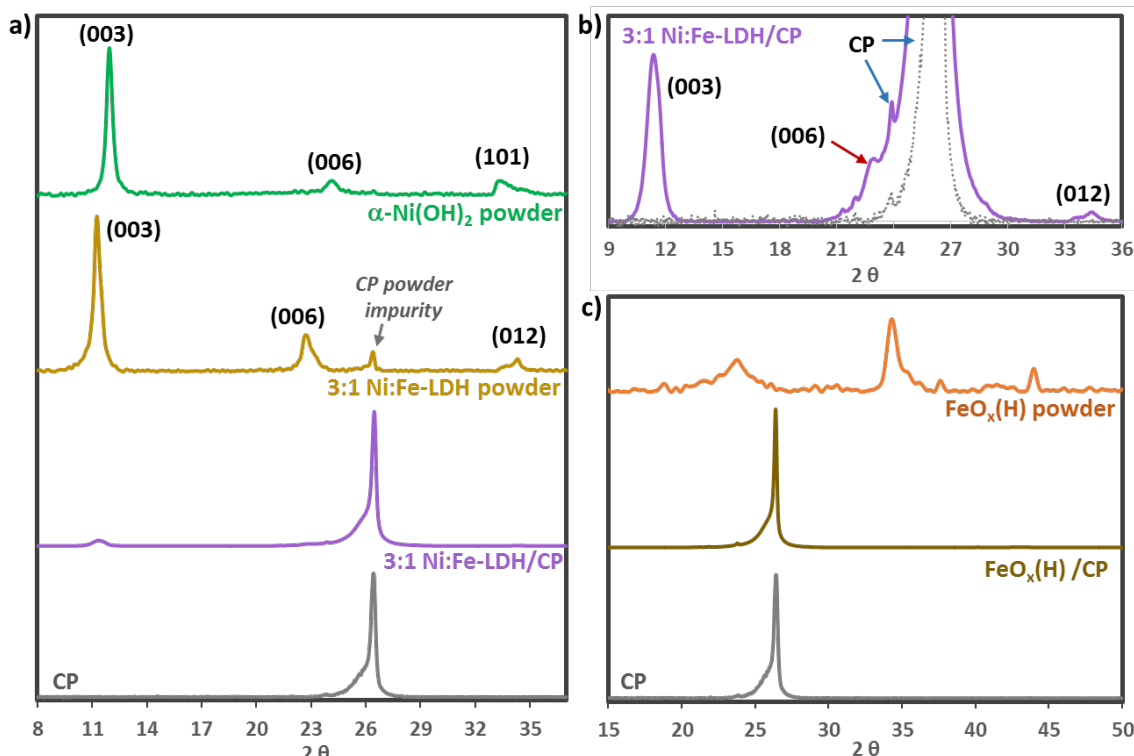


**Figure S4.** (a) Powder X-ray diffraction (PXRD) patterns of the NiFe-LDH catalyst precursor as free powder (yellow trace) and on carbon paper (purple trace and further highlighted in b) showing basal plane peaks at  $2\theta = 11.3^\circ$  for the (003) plane and  $2\theta = 22.6^\circ$  for the (006) plane, confirming the presence of the layered structure. These patterns are consistent with those reported in the literature.<sup>S3</sup> Pattern of a Ni-only sample (green trace) prepared using identical method matches that of  $\alpha$ -Ni(OH)<sub>2</sub> (JCPDS card 38-0715) (c) PXRD pattern for the Fe-only catalyst on carbon paper displayed no obvious diffraction peaks (brown trace). Efforts to match the pattern of the iron oxide powder obtained (orange trace) with various phases of Fe<sub>2</sub>O<sub>3</sub>, Fe<sub>3</sub>O<sub>4</sub>, and  $\alpha$ -,  $\beta$ -,  $\gamma$ -,  $\delta$ -FeOOH were unsuccessful due to the ill-defined nature of the peaks observed.

### 3.2 SEM Imaging and EDX elemental analysis

SEM images of the 3:1 NiFe-LDH catalyst precursor showed thin hexagonal plates vertically attached to the fibers of the carbon paper (Fig. S5). EDX analysis of 20-30 small areas over the entire catalyst deposit showed a Ni:Fe ratio of ~3:1 (Table S1) and no phase segregation was evident by EDX mapping (Fig. S6). SEM images of the 100% hydrous Fe oxide catalyst precursor on CP showed nets of needles horizontally attached to the fibers of the CP, as well as some thin plates vertically attached to CP (Fig. S5b and insets). EDX analyses (Table S1) over the entire deposited area confirmed that only Fe and O are present (and carbon from CP).

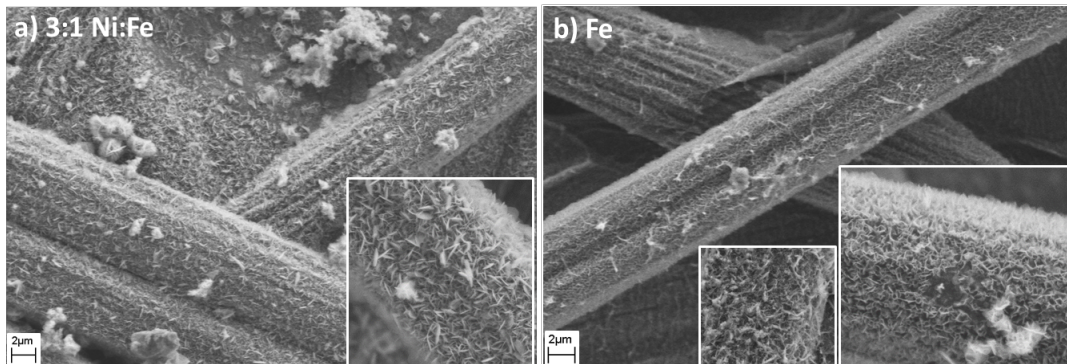


**Figure S5.** SEM images of 3:1 NiFe-LDH and 100% hydrous Fe oxide catalyst precursors on carbon paper. Enlarged insets provide the detailed morphology of each catalyst. It is interesting to note that in the 100% Fe sample, two different fine morphologies (needles and sheets) can be observed.

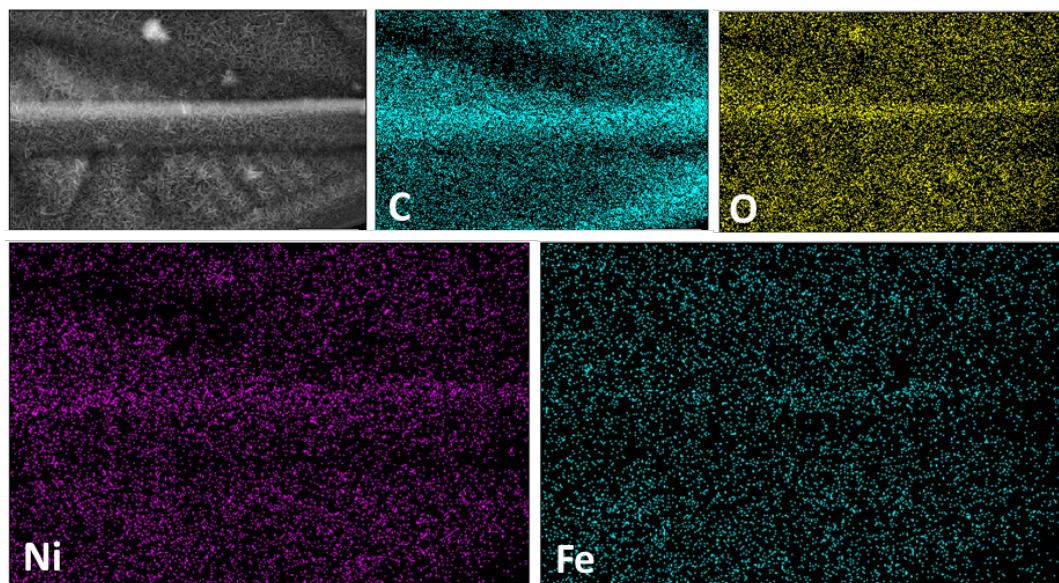


**Figure S6.** EDX elemental mapping of the 3:1 Ni:Fe-LDH catalysts precursor showing no evidence of phase segregation.

#### IV. Mössbauer Results and Parameters

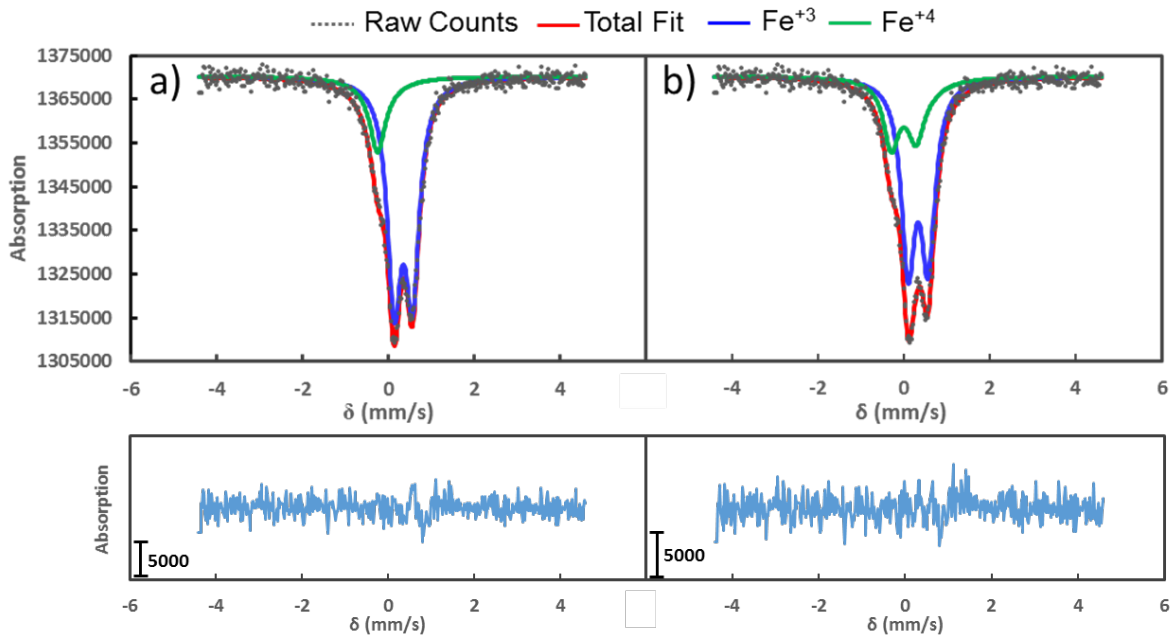


**Figure S7.** Two sets of parameters were found to produce reasonable fit for the  $\text{Fe}^{+4}$  specie. One consist of fitting the new species as a doublet with an isomer shift near zero (a). Alternatively, a singlet with an isomer shift at around -0.25 mm/s and a quadrupole splitting of ~0.6 mm/s (b) also provided a good fit. Lower panel shows the difference spectrum between total fit and the sum of  $\text{Fe}^{+3}$  and  $\text{Fe}^{+4}$  fits for each type of fitting, demonstrating that good fit is obtained in both cases.

**Table S2.** Mössbauer Parameters for Layered 3:1 NiFe Oxyhydroxide Catalyst

3:1 Layered NiFe Oxyhydroxide									
	Site 1 ( $\text{Fe}^{+3}$ )				Site 2 ( $\text{Fe}^{+4}$ )				$\chi^2$
	% Comp	IS	QS	Width	% Comp	IS	QS	Width	
No $E_{\text{app}}$ - start	1	0.34	0.5	0.44					1.13
1.49 V	1	0.34	0.49	0.42					0.99
1.62 V ( $\text{Fe}^{+4}$ as singlet)	0.885	0.34	0.46	0.39	0.115	-0.27	0	0.415	0.91
1.62 V ( $\text{Fe}^{+4}$ as doublet)	0.796	0.34	0.46	0.39	0.204	-0.007	0.59	0.415	0.92
1.76 V ( $\text{Fe}^{+4}$ as singlet)	0.794	0.34	0.46	0.39	0.206	-0.25	0	0.415	1.12
1.76 V ( $\text{Fe}^{+4}$ as doublet)	0.678	0.34	0.46	0.39	0.322	0.004	0.58	0.415	1.09
1.49 V_2 <sup>nd</sup> ( $\text{Fe}^{+4}$ as singlet)	0.803	0.34	0.46	0.39	0.197	-0.23	0	0.415	1.14
1.49 V_2 <sup>nd</sup> ( $\text{Fe}^{+4}$ as doublet)	0.686	0.34	0.46	0.39	0.314	0.012	0.56	0.415	1.13
No $E_{\text{app}}$ - end	1	0.34	0.48	0.485					5.88

**Table S3.** Mössbauer Parameters for the Hydrous Fe-oxide Catalyst.

Hydrous Fe Oxide									
	Site 1 ( $\text{Fe}^{+3}$ )				Site 2 ( $\text{Fe}^{+3}$ with coalescing magnetism)				$\chi^2$
	% Comp	IS	QS	Width	% Comp	IS	QS	Width	
No $E_{\text{app}}$ -start	0.395	0.36	0.65	0.542	0.602	0.53	0	6.35	1.02
1.49 V	0.31	0.37	0.65	0.542	0.689	0.37	0	8.62	1.03
1.62 V	0.322	0.37	0.64	0.542	0.673	0.48	0	6.97	1.10
1.76 V	0.29	0.36	0.65	0.542	0.71	0.55	0	6.12	0.98
No $E_{\text{app}}$ -end	0.355	0.36	0.64	0.52	0.645	0.35	0	5.35	1.42

## References

- S1. Electrodeposition was carried out following the method reported by: Louie M. W.; Bell, A. T. *J. Am. Chem. Soc.*, **2013**, *135*, 12329-12337.
- S2. Brownson, J. R. S.; Lévy-Clément, C. *Phys. Status Solidi B* **2008**, *245*, 1785
- S3. Kim, K. S.; Winograd, N. *Surf. Sci.* **1974**, *43*, 625.
- S4. a) Abellán, G.; Coronado, E.; Martí-Gastaldo, C.; Pinilla-Cienfuegos, E.; Ribera, A. *J. Mater. Chem.* **2010**, *20*, 7451-7455. (b) Gong, M.; Li, Y.; Wang, H.; Liang, Y.; Wu, J. Z.; Zhou, J.; Wang, J.; Regier, T.; Wei, F.; Dai, H. *J. Am. Chem. Soc.*, **2013**, *135*, 8452. (c) Song, F.; Hu, X. *Nat. Commun* **2014**, *5*, 4477.